J|A|C|S ARTICLES

Published on Web 10/01/2009

Stability of Asymmetric Lipid Bilayers Assessed by Molecular Dynamics Simulations

Santi Esteban-Martín,[†] H. Jelger Risselada,[‡] Jesús Salgado,[†] and Siewert J. Marrink*,[‡]

Instituto de Ciencia Molecular, Universitat de València. Polígono La Coma, s/n. 46980 Paterna (Valencia), Spain, and Groningen Biomolecular Sciences and Biotechnology Institute & Zernike Institute for Advanced Materials, University of Groningen, The Netherlands

Received June 2, 2009; E-mail: s.j.marrink@rug.nl

Abstract: The asymmetric insertion of amphiphiles into biological membranes compromises the balance between the inner and outer monolayers. As a result, area expansion of the receiving leaflet and curvature strain may lead to membrane permeation, shape changes, or membrane fusion events. We have conducted both atomistic and coarse-grained molecular dynamics simulations of dipalmitoyl-phosphatidylcholine (DPPC) bilayers to study the effect of an asymmetric distribution of lipids between the two monolayers on membrane stability. Highly asymmetric lipid bilayers were found to be surprisingly stable within the submicrosecond time span of the simulations. Even the limiting case of a monolayer immersed in water ruptured spontaneously only after at least 20 ns simulation. A thermal shock could destabilize these kinetically trapped states. We also studied mixed systems composed of DPPC and short tail diC_8PC lipids, showing that the presence of the cone-shaped short tail lipid facilitates the release of tension in the asymmetric systems via formation of a transmembrane pore. Thus, asymmetric area expansion and curvature stress cooperate to yield bilayer disruption. It appears that, although asymmetric area expansion destabilizes the bilayer structure, the activation energy for transmonolayer lipid re-equilibration is increased. Such a large kinetic barrier can be reduced by lipids with positive spontaneous curvature. These effects are important at the onset of bilayer destabilization phenomena, such as lipid pore formation and membrane fusion, and should be considered for the mechanism of induction of such processes by peptides and proteins.

Introduction

Although lipids in an aqueous environment arrange predominantly as planar bilayer membranes, insertion of some types of amphipathic molecules, such as surfactants and peptides, affects the stability of the lamellar structure, and may thus promote the formation of pores,[1−9] increase the probability of membrane fusion,[10,11] or facilitate phase changes.[12−14] Such asymmetric uptake phenomena are related to the defense and attack mechanisms of cells, as in the case of antibiotic peptides which accumulate in the outer monolayer of bacterial plasma membranes and kill the cell upon permeation.[15−18] Area asymmetry effects also play a role for the fusion of viruses with target cells, mediated by the insertion of fusion peptides into membranes.[19] In some cases, at sufficiently high concentrations of the foreign molecules, their interaction with phospholipid bilayers may lead to solubilization, via the formation of mixed lipid−amphiphile micelles.[20−25] At subsolubilizing levels, binding of amphiphiles to the externally accessible monolayer of lipid vesicles gives

[†] Universitat de València.
[‡] University of Groningen.

(1) Heerklotz, H. *Biophys. J.* **2001**, *81*, 184–95.
(2) Matsuzaki, K.; Murase, O.; Fujii, N.; Miyajima, K. *Biochemistry* **1995**, *34*, 6521–6.
(3) Huang, H. W. *Biophys. J.* **2009**, *96*, 3263–3272.
(4) Tamba, Y.; Yamazaki, M. *J. Phys. Chem. B.* **2009**, *113*, 4846–4852.
(5) García-Sáez, A. J.; Coraiola, M.; Dalla Serra, M.; Mingarro, I.; Menestrina, G.; Salgado, J. *Biophys. J.* **2005**, *88*, 3976–90.
(6) Wieprecht, T.; Apostolov, O.; Beyermann, M.; Seelig, J. *Biochemistry* **2000**, *39*, 442–52.
(7) Allende, D.; Simon, S. A.; McIntosh, T. J. *Biophys. J.* **2005**, *88*, 1828–37.
(8) De la Maza, A.; Parra, J. L. *Biochem. J.* **1994**, *303* (Pt 3), 907–14.
(9) Huang, H. W. *Biochemistry* **2000**, *39*, 8347–52.
(10) Martin, I.; Defrise-Quertain, F.; Decroly, E.; Vandenbranden, M.; Brasseur, R.; Ruysschaert, J. M. *Biochim. Biophys. Acta* **1993**, *1145*, 124–33.
(11) Epand, R. M.; Epand, R. F. *Biochem. Biophys. Res. Commun.* **1994**, *202*, 1420–1425.
(12) Schwarz, S.; Haest, C. W.; Deuticke, B. *Biochim. Biophys. Acta* **1999**, *1421*, 361–79.
(13) Rauch, C.; Farge, E. *Biophys. J.* **2000**, *78*, 3036–47.
(14) Sackmann, E.; Duwe, H. P.; Engelhardt, H. *Faraday Discuss. Chem. Soc.* **1986**, 281–90.
(15) Zasloff, M. *Nature* **2002**, *415*, 389–95.
(16) Wieprecht, T.; Beyermann, M.; Seelig, J. *Biochemistry.* **1999**, *38*, 10377–87.
(17) Vogt, B.; Ducarme, P.; Schinzel, S.; Brasseur, R.; Bechinger, B. *Biophys. J.* **2000**, *79*, 2644–56.
(18) Uematsu, N.; Matsuzaki, K. *Biophys. J.* **2000**, *79*, 2075–83.
(19) Longo, M. L.; Waring, A. J.; Gordon, L. M.; Hammer, D. A. *Langmuir* **1998**, *14*, 2385–2395.
(20) Ollivon, M.; Eidelman, O.; Blumenthal, R.; Walter, A. *Biochemistry* **1988**, *27*, 1695–703.
(21) Keren-Zur, M.; Beigel, M.; Loyter, A. *Biochim. Biophys. Acta* **1989**, *983*, 253–8.
(22) da Graça Miguel, M.; Eidelman, O.; Ollivon, M.; Walter, A. *Biochemistry* **1989**, *28*, 8921–8.
(23) Levy, D.; Gulik, A.; Seigneuret, M.; Rigaud, J. L. *Biochemistry* **1990**, *29*, 9480–8.
(24) Almog, S.; Litman, B. J.; Wimley, W.; Cohen, J.; Wachtel, E. J.; Barenholz, Y.; Ben-Shaul, A.; Lichtenberg, D. *Biochemistry* **1990**, *29*, 4582–92.

 10.1021/ja904450t CCC: $40.75

rise to initially asymmetric distributions between the two leaflets. Although most neutral detergents can easily equilibrate through translocations across the bilayer, it is known that some remain bound asymmetrically.[1,26]

The asymmetric insertion of molecules into lipid vesicles involves an area expansion of the accessible (outer) monolayer, which is also often accompanied by positive-curvature strain. Beyond a certain limit of incorporation, the energy stored can be sufficient to drive the reorganization of the membrane lipids, leading to permeabilization and translocation of molecules to the inner monolayer. For instance, it has been hypothesized that this is the major driving force for the mode of action of certain antimicrobial peptides,[2−4] and theoretical mean field calculations show that the peptides may trigger a phase transition to a porated lamellar state as a direct result of the peptide-induced area expansion.[3] Another example is the effect of bilayer inclusions on the activity of membrane proteins. It has been demonstrated that the large mechanosensitive channel (MscL) can be opened in the absence of external pressure by the asymmetric incorporation of lyso-lipids in the bilayer.[27] The results were interpreted with the hypothesis that such an asymmetric binding of lyso-lipids induces a large local stress and tension on the MscL by changing the local pressure profile in the bilayer.

To shed light on these and related experiments, in this work we investigate the stability and pressure distribution of lipid membranes under conditions of asymmetry of the number of lipids per monolayer and in the presence of inclusions with positive intrinsic curvature. We use atomistic as well as coarse-grained (CG) molecular dynamics (MD) simulations. Despite the biological relevance of asymmetric bilayers, only a few simulation studies have been published so far addressing membrane asymmetry. These include two related studies of the effect of an asymmetric distribution of lipids on the electrostatic potential across the membrane,[28,29] a study addressing how bilayer properties change upon replacing a fraction of PC lipids by charged lipids in one monolayer only,[30] an investigation of the stability of symmetric versus asymmetric membrane domains,[31] and a simulation of the asymmetric adsorption of resorcinolic lipids to a preformed membrane.[32] To the best of our knowledge, no systematic studies about the effect of bilayer asymmetry on bilayer stability have been published so far. Here, we aim to fill this gap. We explore a number of different systems, including pure dipalmitoyl-phosphatidylcholine (DPPC) membranes and mixed bilayers of dioctanoyl-PC (diC_8PC) and DPPC, which we simulate in both symmetric and asymmetric arrangements. In addition, we study the case of addition of the lyso-lipid palmitoyl-PC (PPC) to just one of the two monolayers. The simulations were analyzed in terms of the structural stability of the membranes, and the effect of asymmetry on the order profiles, density distribution, and lateral pressure profiles. The results are presented in the next section, followed by a discussion and details about the methods used.

Results

Asymmetry in a lipid membrane is usually understood as a difference in the chemical composition between the two monolayers. Here, we refer to it primarily as the difference in the number of lipids per leaflet. In systems made of a mixture of lipids, asymmetry refers here also to the composition of each leaflet. This will be clarified for each case. Starting from an equilibrated model membrane with an equal number of DPPC molecules per leaflet, several asymmetric systems were prepared by removing lipids randomly from the lower monolayer (see Methods). For the case of mixed lipid membranes, the excess molecules in the upper monolayer were replaced by short tail diC_8PC lipids or by PPC lyso-lipids. Using these setups, two types of simulations were performed, corresponding to NPT and NP_zAT ensembles. The NPT ensemble mimics a situation where the lipid membrane can freely adjust its area upon inclusion of additional material, whereas the NP_zAT ensemble poses an area constraint. The latter choice reflects the situation in experiments with liposomes, for which the area change is initially restricted by the slow flip-flopping of lipids, before newly incorporated inclusions in the accessible monolayer equilibrate between the two monolayers. Most of the results were obtained with atomistic models, which will be assumed unless otherwise stated in the text. Extended length and time scales were explored using a coarse-grained (CG) model.[33] An overview of all simulations performed is given in Tables 1−3. Since the estimated equilibration times, in terms of area-per-lipid, were in the range of 30−40 ns (see Supporting Information), all analysis were made using the second half of the trajectories.

Asymmetric DPPC Bilayers. For the NPT simulations, upper/lower monolayer lipid ratios of 64/64, 64/54, 64/44, 64/34, and 64/24 were studied, in trajectories up to 70 ns (simulations 1−5, Table 1). In the perturbed asymmetric systems the lower monolayer, with a smaller number of molecules, rapidly rearranged to cover the empty area left by the missing lipids by spreading the hydrocarbon tails of the remaining lipids. Simultaneously, the upper monolayer packed tightly to reduce its area excess with respect to the lower monolayer. Thus, the total area of the membrane diminished, and the corresponding values per lipid molecule for the upper and lower monolayers re-equilibrate to new compressed and expanded values, respectively (Table 1). The deviation from the equilibrium area per lipid is not symmetric, being more pronounced for the expanded leaflet. As expected, the compression of the upper layer increases with the asymmetry of the system, although such compression attenuates at molecule ratios larger than 64/34, approaching a limit value of 0.53 nm^2 for the extreme case with only one monolayer (see below). This trend was quantitatively reproduced in coarse-grained simulations run up to much longer times. (Table 1, simulations 9−13).

The lipid rearrangements in each of the two monolayers strongly affect the bilayer structure. The order parameter profile for a 64/24 asymmetric bilayer (Figure 1A) shows that the acyl chains of lipids in the upper monolayer are better aligned with the bilayer normal, while the chains of lipids in the lower monolayer prefer an almost perpendicular orientation. Moreover, asymmetric density profiles developed, with an increase of

(25) Inoue, T.; Yamahata, T.; Shimozawa, R. *J. Colloid Interface Sci.* **1992**, *149*, 345–358.
(26) Kragh-Hansen, U.; le Maire, M.; Møller, J. V. *Biophys. J.* **1998**, *75*, 2932–46.
(27) Perozo, E.; Kloda, A.; Cortes, D. M.; Martinac, B. *Nat. Struct. Biol.* **2002**, *9*, 696–703.
(28) Gurtovenko, A. A.; Vattulainen, I. *J. Am. Chem. Soc.* **2007**, *129*, 5358–9.
(29) Gurtovenko, A. A.; Vattulainen, I. *J. Phys. Chem. B* **2008**, *112*, 4629–34.
(30) Lopez Cascales, J. J.; Otero, T. F.; Smith, B. D.; Gonzalez, C.; Marquez, M. *J. Phys. Chem. B* **2006**, *110*, 2358–2363.
(31) Bennun, S. V.; Longo, M. L.; Faller, R. *Langmuir* **2007**, *23*, 12465–12468.
(32) Siwko, M. E.; de Vries, A. H.; Mark, A. E.; Kozubek, A.; Marrink, S. J. *Biophys. J.* **2009**, *96*, 3140–3153.
(33) Marrink, S. J.; Risselada, H. J.; Yefimov, S.; Tieleman, D. P.; de Vries, A. H. *J. Phys. Chem. B* **2007**, *111*, 7812–7824.

Table 1. Summary of Properties of Simulated Asymmetric DPPC Bilayers

simulation	ensemble, type	surface tension[a] (mN/m)	lipids per leaflet[a] (upper/lower)	area per lipid (nm^2) (upper/lower)	stability (unperturbed)	stability (after temperature jump)	total simulation time (ns)
1	NPT	0	64/64	0.65/0.65	stable	stable	70
2	NPT	0	64/54	0.61/0.72	stable	stable	70
3	NPT	0	64/44	0.58/0.84	stable	stable	70
4	NPT	0	64/34	0.55/1.04	stable	porated	70
5	NPT	0	64/24	0.55/1.40	stable	porated	70
6 ($2x$, $2y$)	NPT	0	256/96	0.55/1.40	stable	porated	10
7 ($4x$, y)	NPT	0	256/96	0.55/1.40	stable	porated	10
8 ($\times 4$)	NPT	0	64/−	0.53/−[b]	porated/stable[c]	porated	100
9	NPT, CG	0	64/64	0.64/0.64	stable	stable	1000
10	NPT, CG	0	64/54	0.59/0.70	stable	stable	1000
11	NPT, CG	0	64/44	0.57/0.83	stable	stable	1000
12	NPT, CG	0	64/34	0.56/1.05	stable	porated	1000
13	NPT, CG	0	64/24	0.56/1.49	stable	porated	1000
14	NPT, CG	0	256/96	0.56/1.49	stable	porated	500
15	NPT, CG	0	576/−	0.49/−	stable	porated	500
16	$NP_zA^{up}T$	22	64/44	0.65/0.95	stable	stalk-like	70
17	$NP_zA^{up}T$	26	64/34	0.65/1.22	stable	porated	70
18	$NP_zA^{up}T$	26	64/24	0.65/1.73	stable	porated	70
19 ($\times 2$)	$NP_zA^{up}T$	−	64/−	0.65/−	porated	porated	10
20	$NP_zA^{low}T$	−33	64/54	0.55/0.65	stable	stable	70
21	$NP_zA^{low}T$	−26	64/44	0.45/0.65	stable	stable	70

[a] Error bars, obtained from block-averaging using 10 ns windows, are ∼1 mN/m for the surface tension, and less than 1% for the area/lipid. [b] Value corresponding to the metastable (non porated) monolayer (one case out of four). [c] In three cases the simulated monolayer ruptured after 20, 30, and 80 ns. In a fourth case the monolayer remained metastable after the 100 ns simulation.

Table 2. Summary of Properties of Simulated Mixed Symmetric diC_8PC:DPPC Bilayers

simulation	ensemble	type	system (lipids per leaflet: upper/lower)	stability (unperturbed)	total simulation time (ns)
22	NPT	preformed	64diC_8PC/64 diC_8PC	porated	20
23	NPT	preformed	24 DPPC + 40 diC_8PC/24 DPPC + 40 diC_8PC	stable	100
24	NPT	preformed	44 DPPC + 20 diC_8PC/44 DPPC + 20 diC_8PC	stable	100
25	NPT	self-aggregated	128 diC_8PC	worm-like structure	50
26	NPT	self-aggregated	48 DPPC + 80 diC_8PC	worm-like structure	50
27	NPT	self-aggregated	88 DPPC + 40 diC_8PC	worm-like structure	50

Table 3. Summary of Properties of Simulated Mixed Asymmetric diC_8PC:DPPC and PPC:DPPC Bilayers

simulation	ensemble	surface tension[a] (mN/m)	system (lipids per leaflet: upper/lower)	area per lipid[a] (nm^2) (upper/lower)	stability (unperturbed)	total simulation time (ns)
28	NPT	0	44 DPPC + 20 diC_8PC/44 DPPC	0.58/0.84	stable	100
29	NPT	0	34 DPPC + 30 diC_8PC/34 DPPC	−	pore	100
30	NPT	0	24 DPPC + 40 diC_8PC/24DPPC	−	pore	100
31	$NP_zA^{up}T$	18	44 DPPC + 20 diC_8PC/44 DPPC	0.65/0.95	stable	70
32	$NP_zA^{up}T$	−	34 DPPC + 30 diC_8PC/34 DPPC	0.65/1.22	pore	40
33	$NP_zA^{up}T$	−	24 DPPC + 40 diC8PC/24 DPPC	0.65/1.73	pore	20
34	$NP_zA^{low}T$	2	54 DPPC + 10 diC_8PC/54 DPPC	0.55/0.65	stable	60
35	$NP_zA^{low}T$	1	44 DPPC + 20 diC_8PC/44 DPPC	0.45/0.65	stable	60
36	NPT, CG	0	44 DPPC + 20 PPC/44 DPPC	0.50/0.74	stable	1000

[a] Error bars, obtained from block-averaging using 10 ns windows, are ∼1 mN/m for the surface tension, and less than 1% for the area/lipid.

density in the upper layer which becomes tightly packed (Figure 1B). In the systems with largest asymmetry, the expanded lower monolayer leaves space for small gaps which become filled with water molecules, while in the compressed upper monolayer the excess of lipid molecules gave rise to bending deformations or undulations (Figure 2), with some hydrated lipid head groups dragged deep into the bilayer by the high lateral pressure. However, any attempt of these latter lipids to cross the bilayer failed, and no membrane rupture or pore-like structure was found, even for asymmetries as large as ∼60% (simulation 5, Table 1). Therefore, these asymmetric bilayers maintained their integrity during the simulations, with no appreciable transmembrane water diffusion.

To test whether the observed metastability of the asymmetric membranes was a consequence of their small size, we simulated larger systems at conditions of high asymmetry (∼60%) by doubling the x and y dimensions or by a 4 times increase of the x dimension, giving systems with a lipid ratio of 256/96. These were run for 10 ns, with results comparable to the ones described above (simulations 6 and 7, Table 1). In an extreme case, we removed completely one leaflet and simulated the remaining 64 lipids as a single monolayer under NPT conditions. Four independent all-atom simulations were run for 100 ns (simulations 8, Table 1). Surprisingly, the monolayer systems, completely surrounded by water, maintained their integrity at least up to 20 ns simulation (in three cases the monolayer broke at 20, 30, and 80 ns). Even in one case the membrane did not brake after 100 ns simulation, reaching a compression up to 0.53 nm^2 per lipid. However, the rupture events show that although the kinetic barrier for symmetric restoration is high, it can be observed within affordable simulation times at least in the case of the maximum asymmetry.

Larger size scales were probed by means of coarse-grained simulations (Table 1, simulations 14 and 15). Membrane rupture

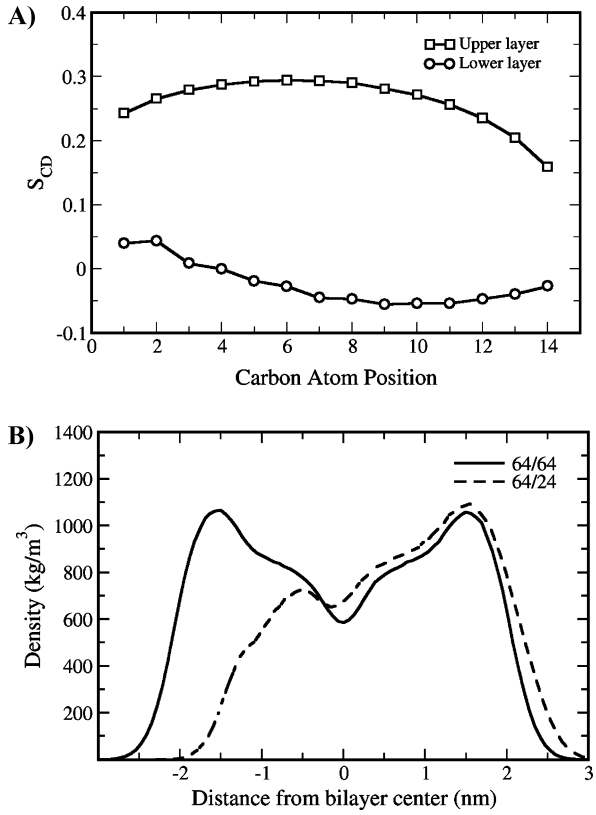

Figure 1. Properties of asymmetric lipid bilayers. (A) Sn1 chain order parameters for an asymmetric DPPC membrane composed of 64 lipids in the upper monolayer (squares) and 24 lipids in the lower monolayer (circles). (B) Global lipid density profiles of simulated symmetric and asymmetric DPPC bilayers. The symmetric system (64 lipids per monolayer) is represented with a solid line and corresponds to simulation 1 of Table 1. The density of the asymmetric bilayer is represented as a dashed line, calculated from simulation 5 of Table 1 (64 and 24 lipids in the upper and lower monolayer, respectively). Upper and lower monolayers correspond to the right and left sides, respectively, of the graphs.

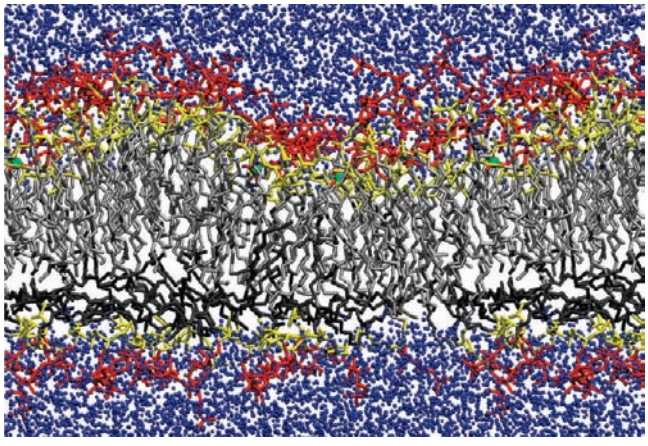

Figure 2. Snapshot of a metastable asymmetric DPPC bilayer (lipid ratio 64/24) after 70 ns (simulation 5, Table 1). The compressed, upper monolayer shows nearly straight acyl chains, forming undulations. In contrast, the lower monolayer is much thinner and leaves space for some water gaps. The acyl chains in this expanded monolayer are very disorganized, often running perpendicular to the membrane normal and in some cases interdigitating with chains of the upper monolayer. Lipid head groups are colored red, the glycerol groups are yellow, and the lipid tails of the upper and lower monolayers are in light and dark gray, respectively. Water is shown as blue spheres. Three choline groups are depicted as green balls to mark lipid head groups pushed into the bilayer as a consequence of overcrowding in the upper monolayer.

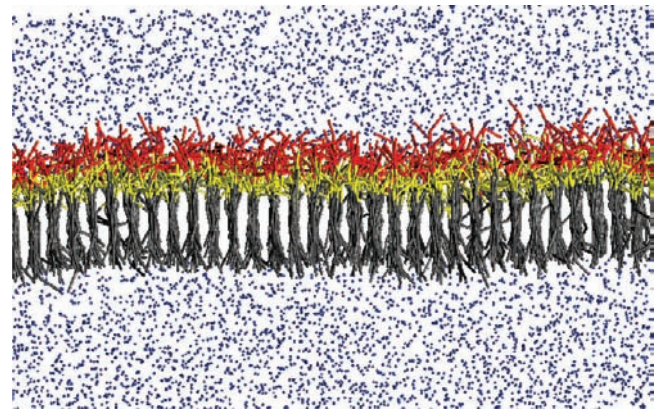

Figure 3. Snapshot of a fully water-immersed coarse-grained DPPC monolayer (simulation 15), which is found to be stable over the simulation time, 1 μs. The monolayer has condensed into a gel phase. Lipid head groups are colored red, the glycerol groups yellow, and the lipid tails gray. Water is shown as small blue dots.

was not observed in any of them, not even for the large single monolayer consisting of 576 lipids (simulation 15). On the basis of the all-atom simulation results, one would expect a nonstable CG monolayer once simulated for a long enough time. However, the CG monolayer remained stable, showing even further compression up to 0.49 nm^2 per lipid (Table 1, simulation 15). Here, the system has adopted a nontilted gel phase. A snapshot obtained at the end of this simulation, showing the fully immersed gel monolayer, is presented in Figure 3. Note that although consistent results were obtained between all atom and CG simulations for most of the systems studied (compare for example the values of area-per-lipid in Table 1), the oversta-bilized CG monolayer may be a consequence of inherent drawbacks of the CG model. In particular, the MARTINI forcefield is known to overestimate, as compared to atomistic simulations,[33] the free energy difference between the equilibrium position of the lipid in the bilayer and the middle of the membrane, which may lead to increased kinetic stabilization of the CG monolayer.

In addition to the NPT ensemble, we performed two different sets of simulations for NP$_z$AT ensembles, where either the upper (NP$_z$A^{up}T) or the lower (NP$_z$A^{low}T) monolayer were kept at their equilibrium area per lipid (referred to a symmetric 64/64 membrane). Here 'upper' refers to the monolayer with excess lipids, and 'lower' to the depleted leaflet. These setups allowed us to emulate states related to the incorporation or release of molecules to, or from, a bilayer under conditions of constant total area. Of note, under NP$_z$AT conditions, for the asymmetric bilayers, a net surface tension term is present (Table 1), which was absent in the NPT ensembles. For the NP$_z$A^{up}T setups, asymmetric membranes with lipid ratios of 64/44, 64/34, and 64/24 were simulated (cases 16−18, Table 1), and no membrane rupture was observed during 70 ns simulation time. However, the complete removal of the lower leaflet permitted the spontaneous formation of a pore after a few nanoseconds (simulations 19, Table 1) in contrast to the behavior of the comparable NPT runs. This pore rapidly facilitates transmembrane lipid re-equilibration to regenerate the missing leaflet and keeps open in the reformed expanded bilayer. For the NP$_z$A^{low}T systems, we studied asymmetries of 64/54 and 64/44 (cases 20 and 21, Table 1), and both kept stable during the simulation time, similarly to comparable NPT runs. Larger asymmetries were not tested because they would force the upper monolayer into unrealistic compression.

The remarkable metastability of largely asymmetric bilayers, at least within our simulation time and conditions, suggests that their relaxation toward equilibrium symmetric systems is kinetically hindered. In agreement with this idea, increasing the temperature up to 500 K for a few picoseconds in systems with a certain minimum asymmetry (~30%) rapidly facilitates molecular reorganization and the appearance of a lipid pore. At the pore wall, the two monolayers get into contact, allowing lateral diffusion of molecules from the compressed to the expanded monolayer, which is followed by pore closure after re-equilibration of the number of lipids. Such a temperature-facilitated relaxation via pore formation was observed for all simulated membranes with an asymmetry ≥64/34.

Mixed diC$_8$PC-DPPC Bilayers. Apart from area expansion, asymmetric insertion of molecules into lipid bilayers is often accompanied by changes in the spontaneous monolayer curvature. In an attempt to understand the contribution of intrinsic curvature of the bilayer molecular components to the disruption of the lamellar structure, mixed systems with DPPC and a lipid with the same headgroup but shorter acyl-chains, diC$_8$PC, were studied (Table 2).

In a first set of simulations, we maintained an equal composition and the same number of lipids (64/64) for the two monolayers in order to evaluate exclusively the effect of the intrinsic positive curvature of diC$_8$PC. Thus, we tested completely symmetric membranes of pure diC$_8$PC and mixtures at diC$_8$PC:DPPC ratios of 80:48 and 40:88 (simulations 22−27, Table 2). The preformed pure diC$_8$PC bilayer (simulation 22) is found to be unstable. The flux of water across this membrane is large compared to a pure DPPC system, and the bilayer finally breaks spontaneously after ~10 ns of simulation. However, for the diC$_8$PC:DPPC mixtures (simulations 23 and 24), no rupture of the bilayer integrity was observed within 100 ns simulation time, although the membrane thickness is clearly reduced. The head groups of both types of lipids are found to be roughly aligned, while the larger DPPC tails spread to cover the space left by the shorter diC$_8$PC tails (Figure 4A). Because these may be kinetically trapped systems, we applied an unbiased alternative strategy to find the most stable lipid-aggregated state, through the simulated self-assembling of all the molecular components. The self-aggregations in water of 128 diC$_8$PC lipids, as well as 80:48 and 40:88 diC$_8$PC:DPPC mixtures (simulations 25−27, respectively, Table 2) yielded highly curved worm-like arrangements in all cases, which formed within 20 ns and kept stable for the rest of the simulation (50 ns).

Asymmetric diC$_8$PC:DPPC systems were prepared by removing lipids only from the lower monolayer of an initially equilibrated DPPC lipid bilayer. The excess lipid molecules in the upper monolayer were then transformed into diC$_8$PC molecules by removing the last eight carbon atoms from each DPPC acyl chain, and simulations corresponding to the NPT and NP$_z$AT ensembles were conducted. The NP$_z$AT runs were performed with either the upper (NP$_z$A^{up}T) or the lower (NP$_z$A^{low}T) monolayer constrained at the equilibrium area per lipid of a reference symmetric bilayer. The different cases studied are summarized in Table 3. For all asymmetry ratios larger than 64/34 (simulations 29, 30, 32, and 33), the bilayers broke spontaneously after a few tens of nanoseconds, in contrast to that observed for analogous pure DPPC asymmetric systems (see above). The spontaneous pore formation and subsequent re-equilibration into a bilayer structure is shown in Figure 5 (simulation 29, Table 3) through different snapshots of this process. For comparison with a symmetric mixed membrane, the density profile of a nonruptured asymmetric mixed bilayer is shown in Figure 4B.

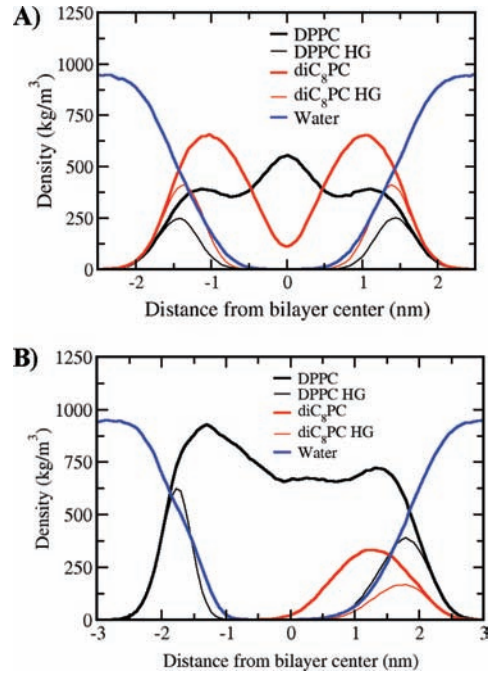

Figure 4. Bilayer density profiles for symmetric and asymmetric diC$_8$PC:DPPC mixed bilayers. (A) Symmetric diC$_8$PC:DPPC mixed bilayer at 80:48 lipid ratio (simulation 23, Table 2). (B) Asymmetric mixed bilayer made of 44 DPPC plus 20 diC$_8$PC lipids in the upper monolayer and 44 DPPC lipids in the lower monolayer (simulation 28, Table 3). Upper and lower monolayers correspond to the right and left sides, respectively, of the graphs. Black and red lines represent density of DPPC and diC$_8$PC molecules, respectively. The blue line corresponds to water molecules. The global densities of lipid atoms are shown as thick lines, and the densities of lipid headgroup atoms are drawn as thin lines.

Effect of Asymmetry on Pressure Profiles. The lateral pressure profile, or stress profile, across a lipid membrane results from the inhomogeneous nature of the interactions within a membrane. As water, head groups, and acyl chains contribute through different forces, one finds the emergence of a nonuniform pressure distribution along the bilayer normal of a lipid bilayer. In biological membranes, this profile has been proposed to be coupled to membrane protein structure and functionality in a manner where changes in the pressure distribution affect protein activation.[34,35] In this section we show how the pressure profile changes for asymmetric membranes. All calculations are based on the CG simulations (simulations 9−13 and 36, Table 1 and 3), for which converging pressure profiles are easily obtained.

Figure 6 shows the lateral pressure profile for a set of pure DPPC bilayers with an increasing asymmetry from 64/64 to 64/24 lipids. At a 64/64 symmetric lipid distribution, the pressure profile is symmetric with respect to the bilayer center. Upon increasing asymmetry, the part of the profile corresponding to the compressed, overpopulated monolayer (negative distances) shows a strong overall increase of pressure, in both the headgroup and tail sections. The pressure increase toward more positive values reflects the intrinsic tendency of the overpopulated and closely packed monolayer to expand. This expansive force, however, is compensated by the contractive pressure

(34) Cantor, R. S. *J. Phys. Chem. B.* **1997**, *101*, 1723–1725.
(35) Brown, M. F. *Chem. Phys. Lipids* **1994**, *73*, 159–180.

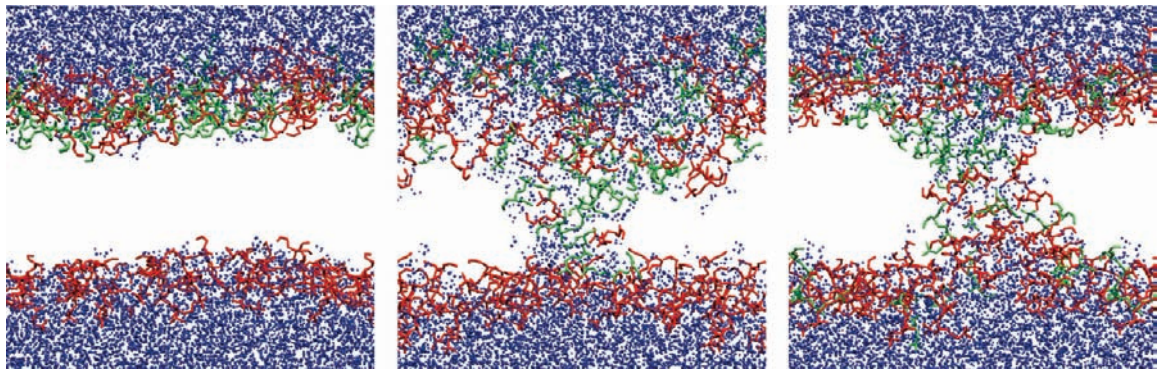

Figure 5. Re-equilibration of a mixed asymmetric bilayer into a mixed and (quasi-) symmetric bilayer through a lipid pore. The figure shows a time series of simulation 29 (Table 3), with snapshots (left to right) at 0 ns, 20 ns (membrane rupture), and 100 ns. DPPC lipid head groups are colored red, and diC_8PC head groups are depicted green. Water molecules are shown as blue spheres. Acyl chains are omitted for clarity.

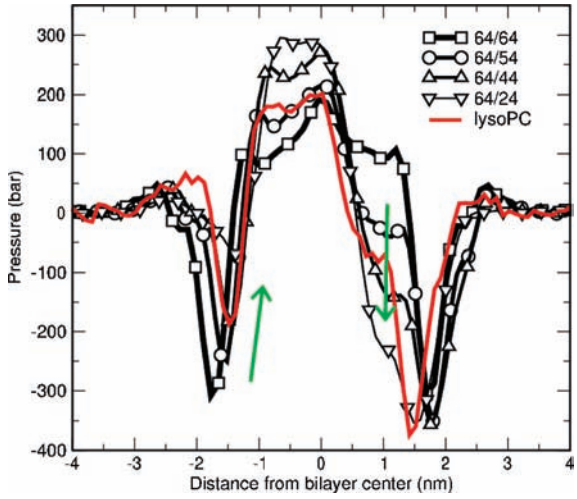

Figure 6. Lateral pressure profiles for coarse-grained, asymmetric DPPC bilayers (simulations 9−11, 13) and DPPC with lyso-lipid PPC added (simulation 36). The bilayer center is at 0 nm, with the overpopulated monolayer located at negative distances. The green arrows point to the effect of increasing the bilayer asymmetry: an increase in pressure for the overpopulated monolayer, and a decrease in pressure for the underpopulated monolayer.

present in the underpopulated monolayer (positive distances). In this part of the profile, especially in the tail region of the lipids, the pressures shift to more negative values. The magnitude of the negative peak coming from the oil−water surface tension located at the interfacial region (at an approximate distance of ±1.7 nm away from the bilayer center) seems only mildly affected by the asymmetry. The integral of the pressure profile is proportional to the surface tension. While the asymmetric bilayers are in a tensionless state (as set by the barostat), the individual monolayers are far from tensionless. For example, the asymmetric depletion or incorporation of around 30% material in one monolayer causes, in the case of pure DPPC (64/44), a surface tension of -22 ± 4 mN/m in the overpopulated and 22 ± 4 mN/m in the underpopulated monolayer.

The asymmetric addition of lyso-lipids (PPC) to the DPPC bilayer has also a strong effect on the pressure profile (Figure 6). However, the qualitative nature of the effect appears similar to the presence of excess DPPC lipids in one of the monolayer leaflets (cf. the 64/44 profile). The induced surface tension in each of the monolayers is also comparable, -18 ± 4 mN/m and 18 ± 4 mN/m in the overpopulated and underpopulated leaflet, respectively.

Discussion

Membrane destabilization phenomena are expected to act at the onset of important biological processes, exerted by membrane active proteins and peptides as part of elementary survival (defense and attack) strategies. Upon asymmetric insertion of foreign molecules within the membrane, stress may arise from the expansion of the accessible outer monolayer with respect to the inner monolayer, and curvature strain depending on the shape of the inclusion and its packing efficiency with the background lipids. As a result, bilayer instability and permeabilization may take place. Because both area expansion and curvature strain may work to destabilize the membrane, a combination of the two should be considered for a realistic mechanism of membrane disruption by the inclusion. Using a minimalistic approach, we have studied the contributions of area expansion and positive-curvature strain to membrane rupture by MD simulations of a number of lipid bilayers with different degrees of asymmetry, made of pure DPPC or a mixture of diC_8PC and DPPC. Note that other mechanisms which may also lead to membrane disruption, such as electroporation, are not considered here.

The energy associated with the insertion of molecules into the lipid membrane depends on the degree of condensation of the bilayer area. If the area is kept constant upon asymmetric insertion, the outer monolayer is compressed by the full cross-sectional area of the incorporated amphiphile. This case is modeled by the $NP_zA^{low}T$ simulations. Alternatively, the release of molecules from one leaflet under constant bilayer area was assessed with the $NP_zA^{up}T$ ensembles. On the other hand, the NPT simulations allow the study of insertion of amphiphiles under zero surface tension. The accumulated tension corresponding to the asymmetric bilayers was expected to be released through membrane rupture, via formation of a lipid pore. For the largest asymmetries, we observed highly perturbed membranes, which include head groups of lipids from the compressed monolayer being dragged toward the interior of the membrane and the appearance of water gaps in the expanded monolayer. However, these systems manifested as remarkably metastable.

The elastic response of lipid bilayers to an applied stress may occur in the form of stretching and compression deformations. In addition, large membrane patches might buckle and bend or even bud-off excess lipids in the form of small vesicles. The latter has been observed in simulations of monolayer compres-

sion, for instance.[36] In our model bilayers, bending is highly suppressed because of the small lipid patches and periodic boundary conditions used in the simulations. Thus, the stored stress is released mainly via stretching and compression deformations. For the NPT ensembles, the systems rearranged by compressing the upper monolayer and expanding the lower monolayer beyond their characteristic equilibrium area per lipid. However, compared to expansion, compression is hindered and cannot proceed beyond a limit. Consequently, area compression and expansion deviations in the respective monolayers are not equivalent. For example, even for the smaller asymmetries (simulations 2 and 3, Table 1), the deviations from the equilibrium area per lipid of the expanded monolayer were larger than those of the compressed monolayer, and close to the maximum compression (simulations 5−7) only expansion is possible.

Related to these observations, vesicle expansion and compression appear to be asymmetric, as far as the thermodynamic driving forces underlying these phenomena are concerned.[37] Additionally, we find that under lipid-number asymmetric conditions monolayer expansion can grow to unexpectedly large values (1.22−1.73 nm^2 for simulations 5−7, 17, 18, Table 1) without apparently affecting the bilayer integrity. This contrasts with the results obtained by simulating the mechanical expansion of a symmetric DPPC bilayer,[38,39] which showed that rupture of the membrane on the submicrosecond time scale takes place after the area per lipid molecule reaches a value of ∼1.20 nm^2. Thus, the bilayer seems to be more resistant to asymmetric than to symmetric expansions (see below). Moreover, it appears that compression of one monolayer may, to some extent, compensate the destabilization tendency due to expansion in the second monolayer. Such compression/expansion readjustments are not possible for the NP_zAT simulations, where instead nonzero surface tension is present. In most cases this was, however, not enough to destabilize the membrane and drive the formation of a pore within the time of the simulations, except for the limit case of completely eliminating the lower monolayer.

The self-assembly of DPPC bilayers from a random distribution of lipids in water produces membranes with small asymmetries (<15%), indicating that large asymmetries are not thermodynamically feasible. Thus, the nonruptured asymmetric systems modeled by our simulations must correspond to kinetically trapped states. In fact, a temperature shock applied to the system (up to 500 K for a few picoseconds) facilitates rupture and re-equilibration of the asymmetric membranes through an intermediate pore state. Nevertheless, this occurs only for asymmetries higher than a relatively large threshold value (∼30%, corresponding to ratios of 64/34 and 64/24). The origin of the barrier which hinders the spontaneous symmetry restoration is the requirement for lipid flip-flops. In a previous simulation study,[40] the free energy barrier associated with lipid flip-flop was calculated to be around 30 kT, and the half-life time of lipids residing in a particular monolayer of the order of minutes to hours. Although this value refers to the case of a symmetric DPPC bilayer, for the asymmetric systems the energy barrier is expected to be even larger, because of the compressed nature of the monolayer containing the excess number of lipids. Thus, while lipid asymmetry destabilizes the bilayer and should promote re-equilibration via lipid flip flop events, the accompanying increase of pressure in the compressed monolayer raises the energy barrier for lipid trans-bilayer reorganization (Figure 7). Although in a long time range lipid re-equilibration will take place, such an effect may have implications for the capacity of biological membranes to buffer transient asymmetries (i.e., incorporation or release of molecules) without compromising membrane integrity.

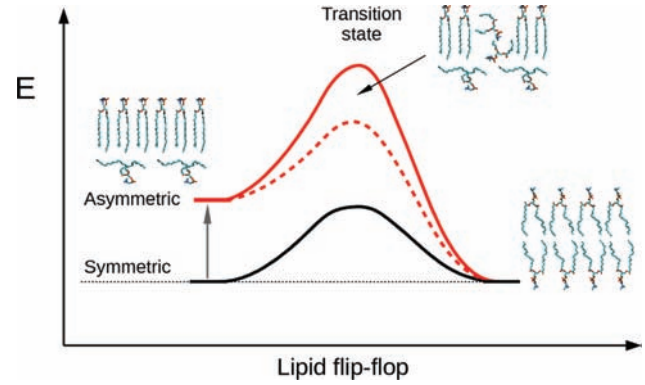

Figure 7. Schematic free energy profiles for lipid flip-flop reorganization in symmetric and asymmetric bilayers. Lipid re-equilibration via pore-mediated flip-flop (transition state) is hindered by a large activation energy. The asymmetric insertion of lipids destabilizes the bilayer (gray arrow) and favors lipid re-equilibration. However, such a destabilization is accompanied by monolayer compression which increases the kinetic barrier in the asymmetric bilayer (red curve). The asymmetric insertion of lipids with intrinsic positive curvature destabilizes the bilayer and reduces the energy barrier for trans-bilayer lipid transfer (red dashed curve), as it facilitates the formation of transient lipid pores. The drawings representing the asymmetric (left), transition state (center) and symmetric bilayers (right) were made by hand just for illustrative purposes.

Frequently, the shape of foreign molecules incorporated into an accessible monolayer differs from the shape of the bulk bilayer components. This gives rise to inefficient molecular packing which affects the intrinsic monolayer curvature. For instance, cone-shaped surfactants, such as lyso-lipids, and lipids with short acyl chains, such as diC_8PC, will not pack well with cylindrically shaped, large acyl-chain DPPC lipids in a planar bilayer environment. They are thus said to possess spontaneous positive curvature and are expected to destabilize the lamellar membrane by promoting the formation of positively curved structures, such as transmembrane pores. We have tested the influence of such curvature effects on membrane disruption by simulating mixed diC_8PC:DPPC systems. The tendency of diC_8PC to stabilize curved structures is demonstrated in self-aggregation studies (simulations 25−27), where in the presence of a relatively large proportion of this lipid, worm-like structures are formed. However, the appearance of such curved structures seems to be kinetically hindered, since they were not observed when we started from preformed symmetric mixed bilayers with a large proportion of diC_8PC (simulations 23 and 24). Finally, the combination of both asymmetric area expansion and curvature effects in asymmetric mixed diC_8PC:DPPC bilayers favored the rapid and spontaneous (with no need of heating) formation of pores for asymmetries larger than 30% (simulations 29, 30, 32, and 33). Therefore, a curved molecular morphology helps to lower the kinetic barriers opposing pore formation (Figure 7) and facilitates the reorganization of asymmetric bilayers once a certain tension threshold is reached due to

(36) Baoukina, S.; Monticelli, L.; Risselada, H. J.; Marrink, S. J.; Tieleman, D. P. *Proc. Natl. Acad. Sci. U.S.A.* **2008**, *105*, 10803–8.
(37) Nebel, S.; Ganz, P.; Seelig, J. *Biochemistry* **1997**, *36*, 2853–9.
(38) Tieleman, D. P.; Leontiadou, H.; Mark, A. E.; Marrink, S. J. *J. Am. Chem. Soc.* **2003**, *125*, 6382–3.
(39) Leontiadou, H.; Mark, A. E.; Marrink, S. J. *Biophys. J.* **2004**, *86*, 2156–64.
(40) Tieleman, D. P.; Marrink, S. J. *J. Am. Chem. Soc.* **2006**, *128*, 12462–12467.

asymmetric area expansion. In line with these results, permeabilization upon asymmetric uptake of detergent molecules has been observed, using isothermal titration calorimetry, for surfactant/lipid ratios in the 20−40% interval.[1] In contrast, micropipet aspiration experiments show that symmetric stretching of bilayers due to vesicle inflation leads to mechanical failure already at 5% area expansion.[41] This, again, implies that the bilayer tolerates asymmetric expansions to a much larger extent than symmetric expansions, which suggest important differences between both phenomena.

The asymmetric bilayer expansion has a clear effect on the distribution of stress throughout the membrane, as illustrated by the pressure profiles (cf. Figure 6). Because of the incorporation of excess lipids in one of the monolayers, the overpopulated monolayer is under negative tension (i.e., wants to expand), whereas the underpopulated monolayer experiences positive tension (i.e., wants to contract). It is of interest to make a comparison between the tensions induced by the asymmetric incorporation of lipids and by the gating threshold of mechanosensitive channels. The latter is reported to be in the range of 8−10 mN/m in the case of Eco-MscL.[42] For our 64/44 bilayer system, the tension in the underpopulated monolayer is already more than 20 mN/m, by far exceeding the gating threshold of the MscL channel, assuming that the gating threshold originates from the so-called constriction region residing at the cytoplasmic side of the membrane. In other words, by incorporation of lipids to the periplasmic side of the membrane, it is possible to create enough tension in the cytoplasmic side to trigger the gating of the channel. This has been shown convincingly in experiments where opening of the channel was observed after the addition of lyso-lipids to reconstituted Eco-MscL.[27] A similar effect has been reported for mechanogated potassium channels.[43] On the basis of the similarity of the pressure profiles and monolayer tensions obtained for the systems with excess DPPC lipids and additional PPC lyso-lipids, we argue that it is not so much the intrinsic curvature of the lyso-lipids which is important but merely the excluded volume effect of the incorporated molecule. Any bilayer inclusion would have a similar effect, a prediction which could be verified experimentally.

Conclusions

We performed a systematic study of the effect of bilayer asymmetry on its properties, including bilayer stability and lateral pressure profile. Asymmetry was achieved by allowing excess lipids in one of the monolayers. Symmetric systems were also considered for comparison. We found that asymmetric DPPC and symmetric mixed short tail/long tail (diC_8PC:DPPC) bilayers keep kinetically trapped into nonruptured states for the time of the simulations (up to 100 ns at the atomistic level, and up to 1 μs at a coarse-grained level of resolution), even for lipid number asymmetries as large as 100% and in the presence of up to 65% diC_8PC, respectively. In contrast, mixed diC_8PC:DPPC systems with the same level of asymmetry ($\geq$30%) spontaneously equilibrate via pore formation. Thus, the present study shows that area expansion and curvature effects cooperate to release bilayer stress through a mechanism involving bilayer poration.

Methods

Simulation Details. All simulations were performed using the GROMACS suite of programs, version 3.1.2.[44] The united atom lipid parameters were adapted from the work of Berger and co-workers,[45] available in electronic form at http://moose.bio.ucalgary.ca/files/lipid.itp. For water, the SPC model[46] was used. Periodic boundary conditions were used with constant pressure and temperature. A Berendsen thermostat,[47] with a coupling constant of 0.1 ps, was used. The reference temperature was set to 323 K, well above the phase transition temperature of DPPC (315 K). Both NPT and NP_zAT ensembles were run. Constant pressure was achieved using the Berendsen scheme,[47] with a coupling constant of 1.0 ps and with the reference pressure set to 1 bar. For the NPT ensemble, pressure coupling was applied semi-isotropically. Simulations were run with a 4 fs time step. Bond lengths were constrained using the LINCS algorithm.[48] Short-range electrostatic and Lennard−Jones potentials were cut off at 1.0 nm, and long-range electrostatic potentials were calculated by using the PME algorithm.[49] DPPC has been extensively studied by MD methods using force fields and setups similar to ours.[50,51]

Self-assembly simulations were performed as described in refs 52 and 53. Briefly, lipid molecules were randomly distributed in the simulation box. The system was then solvated and energy minimized. The production run was performed by allowing the system to evolve freely under anisotropic pressure coupling.

For the coarse-grained simulations, we used the Martini coarse-grained model and associated simulation protocol.[54,33] Topologies for DPPC and the lyso-lipid PPC are available at http://md.chem.rug.nl/~marrink/coarsegrain.html. The same temperature and pressure conditions as for the atomistic level simulations were used. The CG studies only addressed the NPT ensemble.

System Setup. For the atomistic, preformed lipid bilayer simulations, initial coordinates for the DPPC molecules were taken from http://moose.bio.ucalgary.ca/. The system, composed of 128 DPPC lipids and 3655 water molecules, was equilibrated for 100 ns. The final configuration after equilibration was used as starting point for this work.

In all cases the systems were constructed sequentially. From an equilibrated symmetric DPPC lipid bilayer (ratio 64/64, simulation 1 in Table 1), an asymmetric membrane (ratio 64/54, simulation 2 in Table 1) was prepared by randomly removing lipids from the lower monolayer. The last frame of this trajectory was used to build the next asymmetric lipid bilayer (ratio 64/44, simulation 3 in Table 1), etc. We found, however, that similar results were obtained if all asymmetric cases were prepared by removing lipids directly from the symmetric lipid bilayer or by removing a patch of contiguous lipids.

(41) Olbrich, K.; Rawicz, W.; Needham, D.; Evans, E. *Biophys. J.* **2000**, *79*, 321–7.
(42) Sukharev, S. I.; Sigurdson, W. J.; Kung, C.; Sachs, F. *J. Gen. Physiol.* **1999**, *113*, 525–40.
(43) Maingret, F.; Patel, A. J.; Lesage, F.; Lazdunski, M.; Honoré, E. *J. Biol. Chem.* **2000**, *275*, 10128–33.
(44) Lindahl, E.; Hess, B.; van der Spoel, D. *J. Mol. Model.* **2001**, *7*, 306–17.
(45) Berger, O.; Edholm, O.; Jähnig, F. *Biophys. J.* **1997**, *72*, 2002–13.
(46) Berendsen, H.; Postma, J.; van Gunsteren, W.; Hermans, J. *Intermol. Forces.* **1981**, 331–42.
(47) Berendsen, H.; Postma, J.; van Gunsteren, W.; Dinola, A.; Haak, J. *J. Chem. Phys.* **1984**, *81*, 3684–90.
(48) Hess, B.; Bekker, H.; Berendsen, H. J. C.; Fraaije, J. G. E. M. *J. Comput. Chem.* **1997**, *18*, 1463–72.
(49) Essmann, U.; Perera, L.; Berkowitz, M.; Darden, T.; Lee, H.; Pedersen, L. *J. Chem. Phys.* **1995**, *103*, 8577–93.
(50) Patra, M.; Karttunen, M.; Hyvönen, M. T.; Falck, E.; Lindqvist, P.; Vattulainen, I. *Biophys. J.* **2003**, *84*, 3636–45.
(51) Anezo, C.; de Vries, A.; Holtje, H.; Tieleman, D.; Marrink, S. J. *J. Phys. Chem. B* **2003**, *107*, 9424–33.
(52) Marrink, S. J.; Lindahl, E.; Edholm, O.; Mark, A. E. *J. Am. Chem. Soc.* **2001**, *123*, 8638–9.
(53) Esteban-Martín, S.; Salgado, J. *Biophys. J.* **2007**, *92*, 903–12.
(54) Marrink, S. J.; de Vries, A. H.; Mark, A. E. *J. Phys. Chem. B* **2004**, *108*, 750–760.

Simulations under NP_zAT conditions were run at equilibrium area per lipid for both the upper and lower monolayers. One set of simulations ($Np_zA^{up}T$, simulations 16−19, Table 1) was performed after removing lipids from the lower layer, and thus the upper layer remained at its equilibrium area per lipid. In another set of simulations ($Np_zA^{low}T$, simulations 20−21, Table 1), the initial asymmetric bilayer was pushed until the lower monolayer reached its equilibrium area per lipid. Inclusion of diC_8PC molecules was done by removing the last eight carbon atoms from the sn1 and sn2 tails of randomly selected DPPC molecules. In the asymmetric DPPC bilayers, diC_8PC molecules were created only in the upper monolayer, which contains the excess of lipid molecules.

The convergence of the area-per-lipid was used to establish the equilibration times for the systems studied. Equilibration times ranged between 30 and 40 ns. Thus the analysis was performed using the second half of the trajectories. Note that 'equilibration' here means equilibration of the metastable, asymmetric state.

The coarse-grained simulations were set up in a way analogous to the atomistic simulations, starting from a standard DPPC bilayer coordinate file from http://md.chem.rug.nl/~marrink/coarsegrain.html. See Tables 1−3 for an overview of the simulations performed.

Calculation of Pressure Profiles. Pressure profiles were calculated using the method described by Lindahl et al.[55] Although the pressure components cannot be unambiguously locally distributed, as long as short-range forces dominate (which is intrinsically the case in the CG force field), the particular local assignment procedure appears not to be very important.[56] Bilayer pressure profiles published by other groups[55−58] all show very similar features, close to the profile shown in Figure 6 for the symmetric DPPC bilayer.

Acknowledgment. This work has been supported by grants from the Spanish Ministerio de Ciencia e Innovación (BFU200767097, financed in part by the European Regional Development Fund (ERDF), and FPU fellowship (S.E.)), and from The Netherlands Organisation for Scientific Research (NWO) through the Molecule-to-Cell program. The Servei d'Informàtica de la Universitat de València is acknowledged for access to the TIRANT supercomputer.

Supporting Information Available: One figure showing the evolution of the area per lipid along the simulation trajectory for different lipid asymmetries. This material is available free of charge via the Internet at http://pubs.acs.org.

JA904450T

(55) Lindahl, E.; Edholm, O. *J. Chem. Phys.* **2000**, *113*, 3882–93.
(56) Sonne, J.; Hansen, F. Y.; Peters, G. H. *J. Chem. Phys.* **2005**, *122*, 124903–9.
(57) Gullingsrud, J.; Schulten, K. *Biophys. J.* **2004**, *86*, 3496–509.
(58) Ollila, S.; Hyvonen, M. T.; Vattulainen, I. *J. Phys. Chem. B* **2007**, *111*, 3139–3150.